Interface direct shear tests with novel binders

Alvaro Boiero[1], *Enrique* Romero[1], *Marcos* Arroyo[1], and *Giovanni* Spagnoli[2#]

[1]*Universitat Politecnica de Catalunya, Department of Civil and Environmental Engineering, C. Jordi Girona, 1-3 08034 Barcelona, Spain*
[2]*Sweco, Zeche Katharina 6, 45307 Essen, Germany*
[#]*Corresponding author: giovanni.spagnoli@sweco-gmbh.de; spagnoli_giovanni@yahoo.de*

ABSTRACT

In the offshore/marine environment, foundation elements need to be particularly long or wide in diameter in order to reach a competent bearing stratum through weak, low-strength sediments. The seabed conditions in oil&gas and renewable energy projects can be difficult, and the skin friction produced during driving operations could be insufficient to support the service loads placed on the structures. In this study, low-pressure injections of an acrylate gel and a colloidal silica product were made into reference sand, and interface direct shear tests were conducted under constant stiffness conditions. Conventional ground improvement projects already employ these items. Oedometer tests on untreated sand were used to evaluate the stiffness properties of the sand, which provided the foundation for determining the stiffness in the DST_{CNS} system. At an initial low relative density (Dr_o) of 0.40, Holcim sand samples were generated. This value is thought to be representative of the top zone of normal sediment profiles under offshore settings. Shearing the sand over a steel plate has been done by direct shear experiments conducted under constant normal stiffness conditions. The effects of injection have been compared using pre- and post-grout interface shear tests. The new binders' activity is causing an increase in skin friction, according to the results.

Keywords: grouting; direct shear tests; sand; acrylate; colloidal silica.

1. Introduction

Long and heavy offshore piles have notable transient and cyclic components. Because of their length, the piles are compressible with respect to the surrounding soils, and the mobilization of shaft friction over their length produces their load-carrying capabilities (McClelland and Reifel 1986). For driving offshore piles, high-energy impact hammers are frequently employed.

However, in projects related to oil and gas and renewable energy, the seabed conditions could be challenging enough that the skin friction produced during driving is insufficient to support the service loads placed on the structures. It is usually possible to either increase the size of the foundation (Bellato et al. 2015) or improve the geotechnical properties of the soils by using techniques like jet grouting (Parker et al. 1999), deep-soil mixing (Spagnoli et al. 2016), or electrokinetic (Micic et al. 2003) to address foundation issues caused by difficult seabed conditions.

The use of piles in conjunction with binders has already been considered. The geotechnical behaviour of resin-grouted micropiles, which consist of hollow steel anchor bars coated in hardened resin, was examined by Denies et al. (2019). There was a noticeable increase in friction at the resin-soil interface, they found.

The development of driven-grouted piles in the offshore business began in the 1980s (e.g. Nauroy et al., 1986). These piles are particularly useful in carbonate soils, where the very low skin friction that driven piles mobilize provide significant dangers and expenses (e.g. Doherty et al. 2020).

Driven and grouted piles were installed by employing a cement with a water cement ratio presumably about 0.75 to 4, typical of grouting operations (Satyarno et al. 2014). However, when ordinary Portland cement (OPC) grouting is problematic or impossible, medium-to-fine sands are typically grouted using microfine (MF) cement grouts (Mollamahmutoglu and Yilmaz 2011). MF grouts, however, are limited to a soil permeability value of 10^{-4} m/s (Fraccica et al. 2022).

With the evolution of the material technology different new binders are available, such as colloidal silica (Spagnoli and Collico 2023) or acrylic resins (Karol 2003), as a workable substitute for traditional grouts, which are being used in ground development projects (Spagnoli et al. 2022; Spagnoli and Tintelnot 2022). Aqueous suspensions of nano-metric silica particles prepared from saturated silicic acid solutions (Iler, 1979) provide colloidal silica relevant to ground permeation, which gels at a rate dictated by pH and salt concentration (Bergna and Roberts, 2006). Ion-exchange resin is used to extract alkali from sodium silicate in order to create colloidal silica. The sizes of colloids range from 0.002mm to 0.1mm. The electrical double layer surrounding the colloid surface breaks, causing the colloidal silica to gel by altering the pH and ionic strength of the dispersion. A mass of linked spherical colloids is formed when siloxane radicals (Si-OH) start to condense on the surfaces of the colloids (Liao et al., 2003). When different soil particles collide, the gel is created. The particles move closer to one another as the ionic concentration rises. The gel density, which determines how much strength the soil receives, is directly correlated with the grout's silica concentration (e.g., Salvatore et al.,

2020). Soil particles are bound together and are resistant to deformation by the persistent gel created by CS. In this application, CS binds the individual soil particles and fills the pore spaces (Gallagher et al., 2007). Unlike sodium silicate, which is not thought to be a long-lasting substance (Yonekura, 1994), the gel's structure can remain stable for a very long period because there are no sodium ions in it (Yonekura, 1996).

The same redox catalyst system—triethanolamine and ammonium persulfate—and inhibitor—potassium ferricyanide—are used in all acrylate grouts (Karol, 2003). Because acrylates generally have a low viscosity (Bodocsi and Bowers, 1991), they can be utilized in virgin soils with k-values as low as 10^{-5} m/s (Moseley and Kirsch, 2004), although Fraccica et al. (2022) grouted an acrylate in sand with a k-value of 10^{-6} m/s. Nevertheless, there is scarce information regarding the mechanical properties of acrylate-grouted soils in the literature, with the exception of a few number of laboratory data and in situ testing.

Over a number of direct shear tests under constant stiffness conditions (DST_{CNS}), binders for driven-grouted piles made of colloidal silica and acrylate have been tested for possible use. In fact, the friction angle that corresponds to the critical condition at the soil-pile interface (δ_{sc}) is what controls the frictional resistance at the shaft for sands and silts, according to Jardine et al. (1993) from their investigation of instrumented piles for offshore applications. Thus, for piles subjected to service loads, DST_{CNS} may be the most effective method for estimating the possible consequences of soil dampness and radial stress variations.

2. Materials and methods

2.1. Binders

The Holcim sand was treated with two binders: colloidal silica (CS) and acrylate grout (AG).

The CS product used in this work is an aqueous dispersion (density 1.30Mg/m^3) of silica particles of uniform nanometric size and 40% silica concentration, whose properties are summarized in Table 1. The CS was mixed with a NaCl solution (10% w/w) at a volume ratio of 12% to induce the gelling process.

Table 1. Physical and chemical properties of CS compound and accelerator.

	CS compound	**Accelerator NaCl (10%)**
Colour	Whitish	Colorless
Viscosity (20ºC), η (mPa.s)	~10	~1
Density, ρ (Mg/m^3)	1.30	1.07
pH	9.5 to 9.8	7
SiO_2 concentration (%)	40±1	-

On the other hand, AG compound is a low viscosity acrylic resin with fast reaction time. The binder was obtained by mixing an acrylic resin with its accelerator in a mass fraction of 1%. The resin and the accelerator (Part A) were then mixed, in a volumetric ratio of 1, with water with a hardener (0.35% w/w) (Part B). Table 2 includes the main physical and chemical properties of the different compounds used to form the AG binder.

Table 2. Physical and chemical properties of AG compound, accelerator, part B, and hardener.

	Resin	**Accelerator**	**Part B**	**Hardener**
Colour	Clear	Colorless	White	White
Viscosity (20ºC), η (mPa.s)	~5	~2	~12	-
Density, ρ (Mg/m^3)	1.05	0.93	1.01	2.60

Both products were injected into the Holcim sand sample, according the procedure described in section 2.4.

2.2. Sand and steel disc

A Holcim quartz sand (0.2–0.6 mm, Cu=1.4, Cc=1) was utilized in this study; Figure 1 shows the range of its particle sizes, and Table 3 summarizes its physical and chemical characteristics.

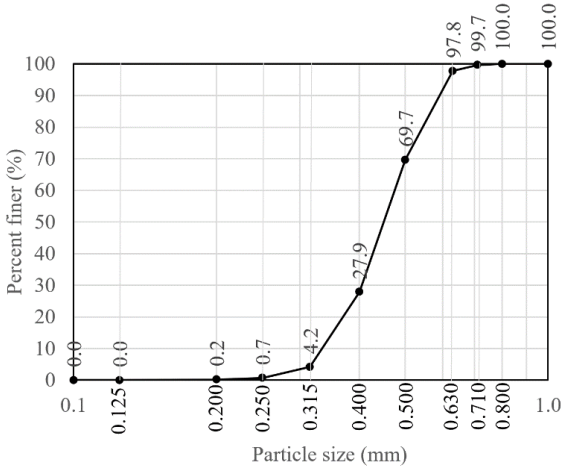

Figure 1. Particle size distribution of Holcim sand (after Boiero et al., 2023).

Table 3. Physical and chemical properties of Holcim sand.

	Value
Effective internal friction angle, ϕ' (º)(*)	38
Mean grain size, d_{50} (mm)	0.450
Density of solids, ρ_s (Mg/m^3)	2.65
Dry density, ρ_d (Mg/m^3)	1.45
Hygroscopic moisture content, w (%)	< 0.3
Maximum void ratio, e_{max}	0.982
Minimum void ratio, e_{min}	0.532
Hydraulic conductivity, k_w (m/s)	7.7x10^{-4}
Stiffness in oedometer, K (kPa/mm)	1500-2000 (**)

(*) Peak strain value from DST under constant normal stress.
(**) For vertical effective stress σ'_v between 60kPa and 810kPa and a sample diameter of 50mm.

A steel disc that was specifically made for this study and has a surface roughness of 26 μm was used for the interaction tests.

2.3. Test set up

A Wykeham Farrance model 27-WF2160 AUTOSHEAR direct shear machine that had been adjusted to meet the constant normal stiffness (CNS) criterion was used for the research. A spring with a known stiffness (KSPRING = 0.5kN/mm), a rod with a base diameter of 60mm (equivalent to the sample's), and a cap that both protects and links the spring to the loading frame work together to produce the CNS state. Furthermore, a redundant 10kN HBM C9C load cell was placed to record any variations in the normal force applied to the specimen during the test. Using data capture software built into the direct shear apparatus, LVDTs and a 5kN horizontal load cell recorded the specimen's vertical and horizontal displacements as well as the shear force during the test

A schematic of the shear box is shown in Figure 2. It displays the locations of the intake holes, where the carbon dioxide was injected, and the outlet holes, where the water that the carbon dioxide had dislodged from the sample pores was retrieved.

A modified protocol proposed by Larsson and Flansbjer (2020) was followed in order to adapt and correct the values of vertical stresses and vertical displacements recorded during the test, taking into account the features of the equipment.

Details of the test set up are provided in Boiero et al. (2023).

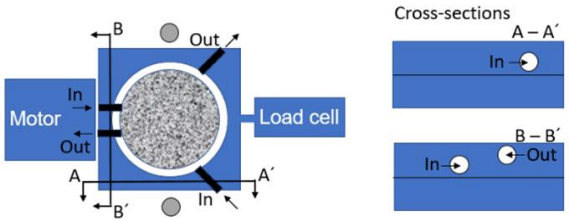

Figure 2. Schematic of the direct shear box

2.4. Sample preparation

At an initial low relative density (Dro) of 0.40, Holcim sand samples were generated. This value is thought to be representative of the top zone of normal sediment profiles under offshore settings. The dry funnel pluviation method was used as part of the sample preparation protocol. The sand samples measured 16.5 mm in height. A 60mm diameter by 23.5mm high steel plate was inserted into the lower section of the shear box for the interaction tests. After that, the sand sample was applied to it using the previously described method.

Once the sample was prepared, the shear box was immersed in water for 30 minutes to reach a high degree of saturation. Subsequently, prior to the injection of the binder, the shear box was covered with a polypropylene membrane to maintain a constant water content condition in the sample. Immediately afterwards, the sample was loaded to generate the initial normal stress (σ_o) prescribed for the test.

For the preparation of the CS binder, the CS suspension was mixed with the accelerating saline solution (Table 1), stirred for 1 minute and permeated into the soil sample previously prepared in the shear box. Permeation occurred through inlet and outlet holes in the upper half of the shear box (Figure 4), pushed by an air-liquid interface system applying an injection pressure of 15kPa. Injection continued until the binder thoroughly permeated the sample. Permeation stopped when a volume of binder corresponding to about 300% of the initial sample void volume flowed out of the upper shear box.

A similar procedure was followed for the case of the AG binder: the resin was mixed with the accelerator (part A), while part B was prepared with the hardener (Table 2). Subsequently, both parts were mixed together until the AG composite was obtained and permeated into the soil sample previously prepared in the shear box. Permeation occurred through inlet and outlet holes in the upper half of the shear box applying an injection pressure of 15kPa, until the binder thoroughly permeated the sample after about 300% of the initial sample void volume flowed out of the upper shear box.

Once the injection stage was completed, the improved sample was subjected to a curing process for 24 hours for AG binder and 60 hours CS binder. Those times was selected to ensure that the binder reaches an unconfined compression strength greater than 80% of the maximum strength accomplished at 28 days of curing, based on available information on curing time and achieved strength published by Fraccica et al. (2022b) and provided by the CS/AG compounds manufacturer.

The sample was then unloaded and put into the direct shear test device. It was not thought that there would be a noticeable volume increase as a result of unloading during the translation of the soil sample from the curing point to the direct shear apparatus because of the granular nature of the sample and the injection and curing procedures.

3. Results and discussion

The DST_{CNS} were performed at three initial normal stresses σ_o=100, 150 and 200kPa, both for CS and AG binders. The horizontal displacement rate was set at 1mm/min, and the tests were extended up to a maximum horizontal displacement D_H of 6mm in all cases. It was also verified that a stable stress condition was reached at D_H = 6mm.

Figures 3 to 8 display the time evolution curves obtained for shear stress τ and normal stress ratio τ/σ_n versus horizontal displacement D_H. Figures 3 and 4 correspond to the untreated sand-steel interface, Figures 5 and 6 correspond to the CS treated sand-steel interface, and Figures 7 and 8 to the AG treated sand-steel interface.

The evolution of the shear stress τ versus normal effective stress σ_n is plotted in Figure 9: untreated sand-steel interface (Fig. 9A); CS treated sand-steel interface (Fig. 9B), and AG treated sand-steel interface (Fig. 9C). The shear-strength failure envelopes (FE) for the sand-steel interfaces (for untreated and treated sand) are also plotted in the figures.

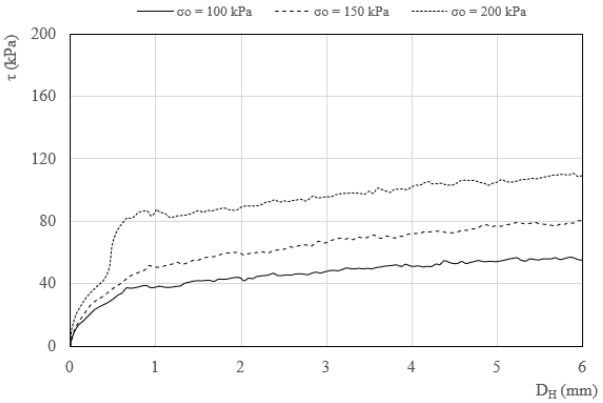

Figure 3. Shear stress vs horizontal displacement for the non-treated sand-steel interface.

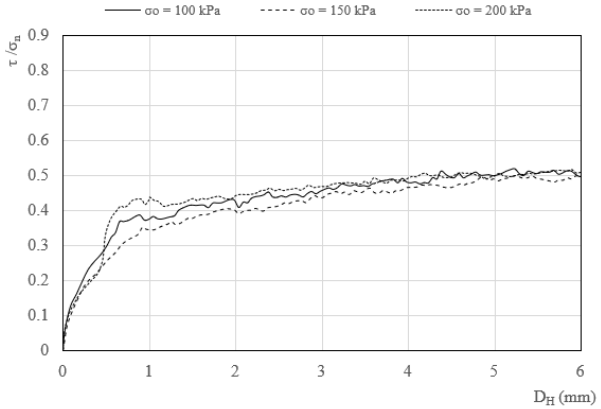

Figure 4. Shear strength/normal stress ratio vs horizontal displacement for the non-treated sand-steel interface.

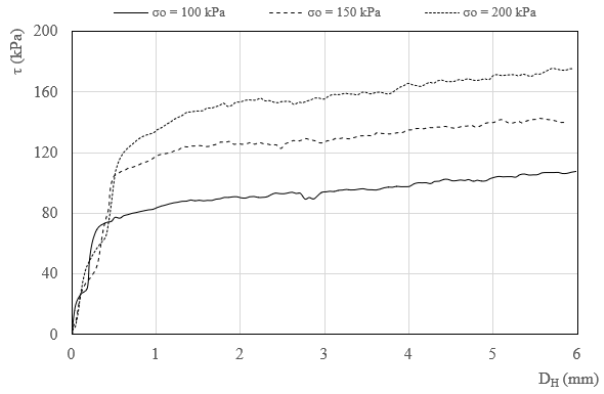

Figure 5. Shear stress vs horizontal displacement for the CS-treated sand-steel interface.

As the previous graphs show, the stress ratio τ/σ_n becomes constant and equal to 0.5 around D_H=4mm for the untreated sand. The same effect is observed for the CS-treated sand, where τ/σ_n reaches a stable value between 0.7 and 0.8 for D_H=3mm, while for AG-treated sand, τ/σ_n reaches a stable value between 0.5 and 0.6 for D_H=3mm. Also, it should be noted that for the AG-treated sand, the τ/σ_n ratio shows a peak around D_H=0.5-1mm, particularly pronounced for an initial vertical pressure of 100kPa. This behaviour could be associated with a higher adhesion in the interface steel-improved sand with resin, which is not observed in the untreated sand nor in the CS-treated sand-steel interfaces.

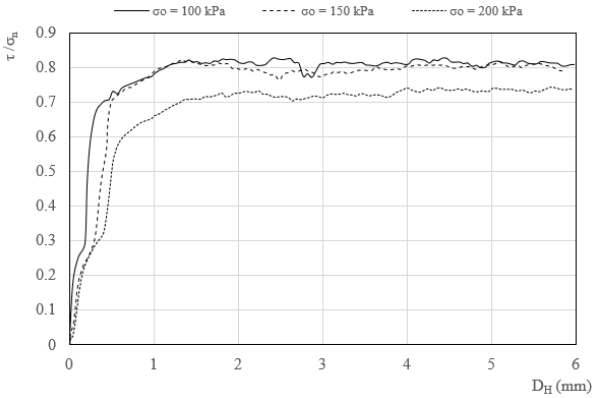

Figure 6. Shear strength/normal stress ratio vs horizontal displacement for the CS-treated sand-steel interface.

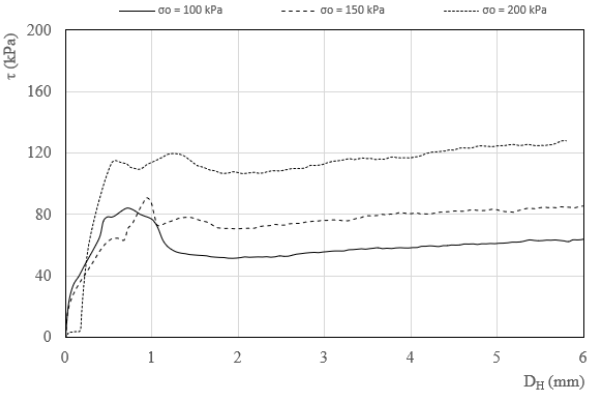

Figure 7. Shear stress vs horizontal displacement for the AG-treated sand-steel interface.

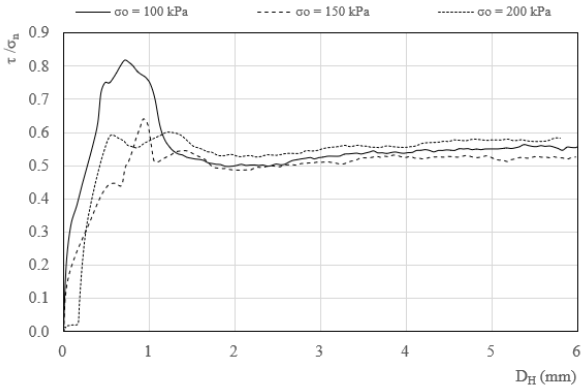

Figure 8. Shear strength/normal stress ratio vs horizontal displacement for the AG-treated sand-steel interface.

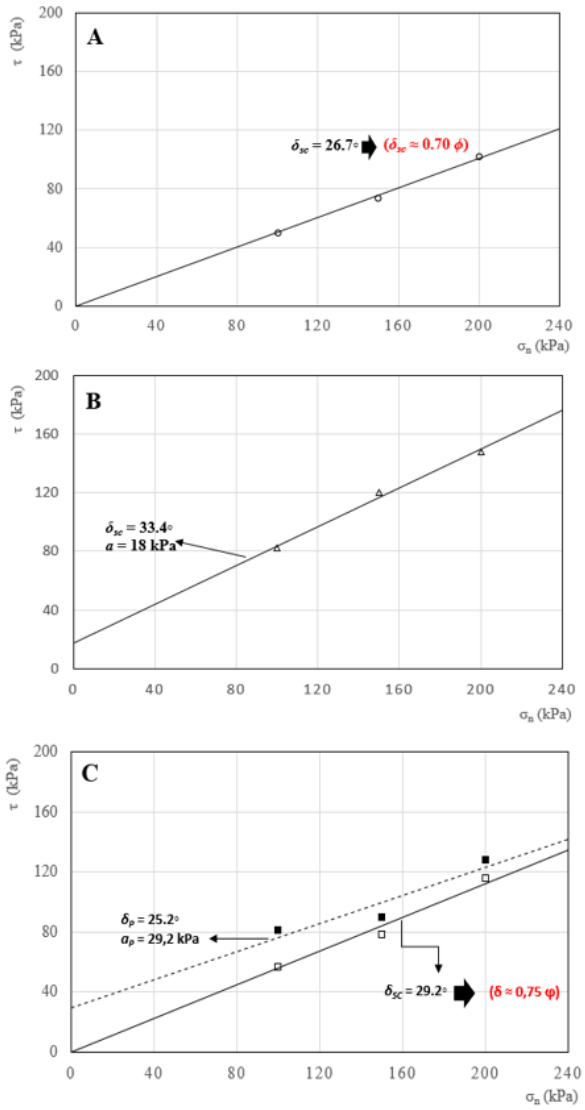

Figure 9. Shear stress vs normal stress failure envelopes for the non-treated sand (A), CS treated sand (B), and AG treated sand.

On the other hand, from the τ-σ_n graph for untreated sand (Figure 9A), the interface friction angle at the ultimate shear strength is δ_{sc}=26.7º (approximately 0.70ϕ', where ϕ' is the effective angle of internal friction of the sand indicated in Table 3). For the CS-treated sand (Figure 9B), the interface friction angle is δ_{sc}=33.4º, with an adhesion soil-steel of about 18kPa. For the case of AG-treated sand (Figure 9C), the ultimate interface friction angle is δ_{sc}=29.2º (about 0.75ϕ'), quite similar to the untreated sand. However, for the peak condition, the interface friction angle is δ_P=25.2º with an adhesion soil-steel of 29kPa, an effect associated with the resin-steel adhesion, as was previously mentioned. Accordingly, it is evident that, for the cases studied in this research, the presence of CS/AG binder increases the ultimate friction angle at the interface by about 9% (with AG compounds) to 30% (with CS compounds), also providing an adhesive component.

From the point of view of offshore applications, the injection of CS/AG-based products would provide increased shear strength at the sand-steel interface, which is particularly beneficial for sedimentary environments with a high content of calcareous soils.

4. Conclusions

Post-grouting interface tests have been performed using novel binders. Direct shear tests under constant stiffness conditions have been performed by shearing the sand over a steel plate, as they are one of the quickest and relatively simple ways to estimate the potential effects of soil dilatancy for piles subjected to service loads. First, grouting under low pressure (15kPa) through several holes in the shear box's upper half was performed. Then, after the curing period of 24 hours (for AG binder) and 60 hours (for CS binder), under loaded conditions, shear tests on the sand-steel interface with and without binders were performed. Results show that the grouting of the novel binders improves the adhesion and friction angle of sand-steel interfaces, allowing the ultimate state condition to be reached for slightly smaller displacements in the case of treated sand. In the particular case of a resin-based binder, a development of an important treated sand-steel adhesion component at the peak strength condition it is observed.

References

Bellato D, Spagnoli G, Wiedenmann U. (2015). Engineering and environmental aspects of offshore soil mixing. Proceedings of the Institution of Civil Engineers-Geotechnical Engineering, 168(GE3): 267–278, http://dx.doi.org/10.1680/geng.14.00044.

Bergna, HE, and Roberts, WO. (2005). Colloidal silica: fundamentals and applications, CRC Press, Boca Raton, FL.

Boiero A, Spagnoli, G, Romero E, and Arroyo M. (2023). Interface direct shear tests simulating post-grouting pile installation with novel binders. Proceedings of the 9th International Conference Offshore Site Investigation and Geotechnics, London UK, 441-446.

Bodocsi, A, and Bowers, MT (1991). Permeability of acrylate, urethane, and silicate grouted sands with chemicals. Journal of Geotechnical Engineering, 117(8):1227-1244, 10.1061/(asce)0733-9410(1991)117:8(1227)

Denies N, Huybrechts, N, de Ruijter, M, Kempenaers, P and Smits D. (2019). In-situ test campaign on innovative resin grouted micropiles. Proceedings of the XVII ECSMGE-2019 Geotechnical Engineering foundation of the future, 10.32075/17ECSMGE-2019-0145.

Doherty, P, Spagnoli G, and Doherty, M (2020). Laboratory investigations to assess the feasibility of employing a novel mixed-in-place offshore pile in calcareous deposits. Ships and Offshore Structures, 15(1):29-38.

Fraccica A, Spagnoli G, Romero E, Arroyo M. and Gomez R. (2022a). Permeation grouting of silt-sand mixtures. Transportation Geotechnics, 35: 100800, https://doi.org/10.1016/j.trgeo.2022.100800.

Fraccica A, Spagnoli G, Romero E, Arroyo M. and Gomez R. (2022b). Exploring the mechanical response of low-carbon soil improvement mixtures. Canadian Geotechnical Journal, 59:726-742, https://doi.org/10.1139/cgj-2021-0087.

Gallagher, PM, Conlee, CT, and Rollins, KM (2007). Full-scale field testing of colloidal silica grouting for mitigation of liquefaction risk. Journal of Geotechnical and

Geoenvironmental Engineering, 133(2):186–196, https://doi.org/10.1061/(ASCE)1090-0241(2007)133:2(186).

Iler R.K. (1979). The chemistry of silica: solubility, polymerization, colloid and surface properties, and biochemistry. Wiley, New York.

Jardine, R., Lehane, B. and Everton, S. (1993). Friction coefficients for piles in sands and silts. Volume 28: Offshore Site Investigations and Foundations Behaviour. 661-677. Society for Underwater Technology. The Netherlands.

Karol, R.H. (2003). Chemical Grouting and Soil Stabilization. Marcel Dekker, Inc., New York, NY.

Larsson, J. and Flansbjer, M. (2020). An approach to compensate for the influence of the system normal stiffness in CNS direct shear tests. Rock Mechanics and Rock Engineering, 53:2185-2199. https://doi.org/10.1007/s00603-020-02051-0.

Liao HJ, Huang CC and Chao BS (2003). Liquefaction resistance of a colloid silica grouted sand. Proceedings of the Third International Conference on Grouting and Ground Treatment, February 10-12, 2003, New Orleans, Louisiana, United States, 1305-1313.

McCleeland, B, and Reifel, M.D. (1986) Planning and Design of Fixed Offshore Platforms. Van Nostrand Reinhold Company Inc., NY.

Micic S, Shang JQ and Lo KY. (2003) Improvement of the loadcarrying capacity of offshore skirted foundations by electrokinetic. Canadian Geotechnical Journal 40(5): 949–963.

Mollamahmutoglu, M, and Yilmaz, Y. (2011). Engineering properties of medium-to-fine sands injected with microfine cement grout. Marine Georesources and Geotechnology, 29(2):95-109, DOI: 10.1080/1064119X.2010.517715.

Moseley, MP, and Kirsch, K. (2004). Ground Improvement. CRC Press, London.

Nauroy, JF, Brucy, F, Le Tirant, P, and Kervadec, JP (1986). Design and installation of piles in calcareous formations. Proc. 3rd International Conference on Numerical Methods in Offshore Piling, Nantes, Ed. Technip, Paris, 461-480.

Parker EJ, Jardine RJ, Standing JR and Jullian X. (1999) Jet grouting to improve offshore pile capacity: GOPAL project. Proceedings of the Offshore Technology Conference, Houston, TX, USA, OTC 10828. http://dx.doi.org/10.4043/10826-MS.

Salvatore E, Modoni, G, Mascolo, MC, Grassi, D and Spagnoli G. (2020). Experimental evidence of the effectiveness and applicability of colloidal nanosilica grouting for liquefaction mitigation. Journal of Geotechnical and Geoenvironmental Engineering, 146(10): 04020108, https://doi.org/10.1061/(ASCE)GT.1943-5606.0002346.

Satyarno, I, Solehudin, AP, Meyarto, C, Hadiyatmoko, D, Muhammad, P, and Afnan, R. (2014). Practical method for mix design of cement-based grout. Procedia Engineering, 95:356 – 365.

Spagnoli G, Scheller P and Doherty P. (2016). In situ and laboratory tests on a novel offshore mixed-in-place pile for oil and gas platforms. Journal of Petroleum Science and Engineering, 145:502–509, https://doi.org/10.1016/j.petrol.2016.06.027.

Spagnoli G (2021). A review of soil improvement with non-conventional grouts. International Journal of Geotechnical Engineering, 15(3): 273-287, https://doi.org/10.1080/19386362.2018.1484603.

Spagnoli G, Seidl W, Romero E, Arroyo M, Gomez R and Lopez J (2021). Unconfined compressive strength of sand-fine mixtures treated with chemical grouts. In: Elshafie M, Viggiani G, and Mair R. (eds.). Geotechnical Aspects of Underground Construction in Soft Ground: Proceedings of the Tenth International Symposium on Geotechnical Aspects of Underground Construction in Soft Ground, IS-Cambridge 2022, Cambridge, United Kingdom, 27-29 June 2022. Boca Raton: CRC Press, 829-835.

Spagnoli G and Tintelnot G (2022a). Mechanical properties of a sand injected with a colloidal silica binder with different dilution grades. International Journal of Geosynthetics and Ground Engineering, 8(47), https://doi.org/10.1007/s40891-022-00391-1.

Spagnoli G and Tintelnot G (2022b). Anwendung von neuartigen niedrigviskosen Bindemitteln für Porenrauminjektionen in feinkörnigen Böden – Grundlagen und Praxisbeispiele. STUVA Forschung + Praxis 58: Forum Injektionstechnik 2022, 16-22.

Spagnoli G, Chittenden N, Grassi D and Cortez JJ (2022). Case histories on the applications of colloidal silica for permeation grouting. DFI-EFFC International Conference on Deep Foundations and Ground Improvement: Smart Construction for the Future, Berlin, Germany, 202-211.

Spagnoli, G., and S. Collico. 2023. “Multivariate Analysis of a Grouted Sand with Colloidal Silica at Different Dilution Stages.” Transp. Geotech 40: 100987, https://doi.org/10.1016/j.trgeo.2023.100987.

Yonekura, R. 1994. “Recent Chemical Grout Engineering for Underground Construction.” Int. Symposium on Anchoring and Grouting Techniques, 7-10 December 1994, 97-113, Guangzhou, China

Yonekura, R. 1996. “The Developing Process and the New Concepts of Chemical Grouting in Japan.” Proceedings of the IS-TOKYO ’96, 2nd International Conference on Ground Improvement Geosystems, Vol. 2, 889-901.